

A kinematic study of planetary nebulae in the dwarf irregular galaxy IC10 ^{*}

Denise R. Gonçalves^{1,2,†}, Ana M. Teodorescu³, Alan Alves-Brito⁴,
Roberto H. Méndez³ and Laura Magrini⁵

¹ *Observatório do Valongo - Universidade Federal do Rio de Janeiro, Ladeira Pedro Antonio 43, 20080-090 Rio de Janeiro, Brazil*

² *Department of Physics and Astronomy, University College London, Gower Street, WC1E 6BT London, UK*

³ *Institute for Astronomy, University of Hawaii, 2680 Woodlawn Drive, HI 96822 Honolulu, USA*

⁴ *Research School of Astronomy and Astrophysics, The Australian National University, Cotter Road, Weston, ACT 2611, Australia*

⁵ *INAF - Osservatorio Astrofisico di Arcetri, Largo E. Fermi 5, I-50125 Firenze, Italy*

20 June 2018

ABSTRACT

We present positions, kinematics, and the planetary nebula luminosity function (PNLF) for 35 planetary nebulae (PNe) in the nearest starburst galaxy IC10 extending out to 3 kpc from the galaxy’s centre. We take advantage of the deep imaging and spectroscopic capabilities provided by the spectrograph FOCAS on the 8.2m Subaru telescope. The PN velocities were measured through the slitless-spectroscopy technique, which allows us to explore the kinematics of IC10 with high precision. Using these velocities, we conclude that there is a kinematic connection between the H I envelope located around IC10 and the galaxy’s PN population. By assuming that the PNe in the central regions and in the outskirts have similar ages, our results put strong observational constraints on the past tidal interactions in the Local Group. This is so because by dating the PN central stars, we, therefore, infer the epoch of a major episode of star formation likely linked to the first encounter of the H I extended envelope with the galaxy. Our deep [O III] images also allow us to use the PNLF to estimate a distance modulus of 24.1 ± 0.25 , which is in agreement with recent results in the literature based on other techniques.

Key words: galaxies: Local Group; galaxies: individual: IC10; galaxies: kinematics and dynamics; ISM: planetary nebulae

1 INTRODUCTION

Even though dwarf galaxies are currently the most abundant galaxy population, and were probably even more abundant during the first epochs of the Universe, the theory of their formation is still under debate (Mateo 1998). According to the hierarchical formation scenario (see, e.g., White & Frenk 1991), they are potential building blocks of larger structures, so their study is crucial for understanding galaxy formation and evolution processes. One of the several questions about their formation and evolution, and that still remains unsolved, is the origin of the differences between the irregular and spheroidal morphological types (see Mateo 1998, for a review). We have been approaching this issue by using planetary nebulae (PNe, old-intermediate stellar population) and

H II regions (young population) as tracers of the chemical evolution of the Local Group (LG) dwarf galaxies (see, for example, Gonçalves et al. 2007; Magrini & Gonçalves 2009; Magrini et al. 2011; Gonçalves et al. 2012). In particular, we have dedicated the last few years in the study of the dwarf irregular galaxy IC10 – its PNe and H II regions (Magrini et al. 2003; Magrini & Gonçalves 2009); its serendipitously discovered symbiotic system, which is the farthest known symbiotic star to date (Gonçalves et al. 2008); and its detailed chemical evolution history (Yin et al. 2010). Here we present a kinematic study of PNe in this galaxy. As a by-product, we also present some photometric results.

IC10 is a dwarf irregular galaxy located in the outskirts of the Local Group at a low galactic latitude ($l = 119^\circ.0$, $b = -3^\circ.3$; NASA/IPAC Extragalactic Database, NED), which makes the reddening values very uncertain. The estimates of the reddening range from $E(B-V)=0.47$ to 2.0, translating into a distance modulus ($m - M$) that varies from 22 to

^{*} Based on data collected at the Subaru Telescope, which is operated by the National Astronomical Observatory of Japan.

[†] E-mail: denise@astro.ufrj.br

more than 27 mag, i.e., the linear distance for IC 10 would vary from 0.5 to 3 Mpc (Sakai, Madore & Freedman 1999; Demers, Battinelli & Letarte 2004). More recent estimates locate IC10 at a distance around 0.7-0.8 Mpc (e.g., Pustilnik & Zucker 2008; Sanna et al. 2008; Kim et al 2009), suggesting a possible membership to the M31 subgroup.

In addition, IC10 has a high star formation rate (SFR) as evidenced by its large number of H II regions (Hodge & Lee 1990) as well as for its H α (Mateo 1998) and far-IR (Melisse & Israel 1994) luminosity. It also has a huge number of Wolf-Rayet stars per unit luminosity, the largest in the LG (Massey, Armandroff & Conti 1992; Massey & Armandroff 1995), and an anomalous ratio of carbon-type Wolf-Rayet stars (WC stars) to nitrogen-type Wolf-Rayet stars (WN stars), which is peculiar at its metallicity (0.2-0.3 solar; cf. Skillman, Kennicutt & Hodge 1989 and Garnett 1990). The presence of an extended and complex H I envelope (Shostak & Skillman 1989, hereafter SS89) suggests that IC10 is still in its formative stage or that it has undergone a major merger episode (Wilcots & Miller 1998, hereafter WM98). Altogether these characteristics suggest that IC10 is experiencing an intense and very recent burst of star formation, likely triggered by infalling gas from its H I envelope which is counter-rotating with respect to the galaxy proper rotation (WM98).

The Local Group Census (cf. Corradi & Magrini 2006) discovered a large number of planetary nebulae (PNe) in many dwarf galaxies, including IC10. Several of these PNe were found at large distances from the centre of their host galaxies, and so could represent a trace of past tidal interactions and/or a connection of the old stellar population with the H I envelope located around some dwarf galaxies, as in the case of IC10 (Huchtmeier 1979).

Single-dish 21 cm observations showed that IC10 is embedded within a huge envelope of H I extending seven times farther than its optical diameter and stretching nearly a degree on the sky (Huchtmeier 1979; Huchtmeier, Seiradakis & Materne 1981). Moreover, the H I velocity field of IC10 appears to be quite complex (Huchtmeier 1979) with a long stream extending to the South of the galaxy. Interferometric data revealed that IC10 has a rotating disk surrounded by a counter-rotating or highly warped outer distribution of gas (SS89).

The most likely scenario is that the gas component represents a late acquisition. Numerical simulations, for example, indicate that mergers can lead to counter-rotating cores (e.g., Thakar et al. 1997). The detection of a stellar population related to the outer envelope would be extremely important to constrain its age and thus the evolution of IC10, dating the possible encounter between the two components. However, so far deep optical images did not show any stellar population coincident with the extended gas envelope, as discussed by WM98 from their examination of Digital Sky Survey and deep WIYN R band images. The surface brightness of this stellar population is expected to be very low, and its detection is strongly limited by scattered light from nearby bright objects and by the contribution of faint discrete sources. These limitations can be circumvented observing PNe because they are easily detectable from their strong nebular emission of [O III] at 5007 Å.

In this paper we aim at studying the radial velocities of the PN population of IC10 in order to explore the connec-

tion of its intermediate to old stellar population with its H I envelope. Previous to the present work, the PN kinematics of this galaxy was never explored, although a number of PNe were already known. Altogether sixteen candidate PNe were identified in IC10 by the Local Group Census in Magrini et al. (2003). Other nine fainter PNe were detected and immediately confirmed using deep spectroscopy by Magrini & Gonçalves (2009).

2 DATA ACQUISITION AND REDUCTION

The observations were made by one of us (R.H.M.) with the Faint Object Camera and Spectrograph (FOCAS; Kashikawa et al. 2002) attached to the Cassegrain focus of the 8.2 m Subaru telescope, Mauna Kea, Hawaii.

2.1 Observations

Data were obtained during a single night, 2010 September 30th. The night was photometric, with an average seeing of 0''.8.

The field of view of FOCAS is 6.5 arcmin and is covered by two CCDs of $2k \times 4k$ (pixel size 15 μm) with an unexposed gap of 5'' between them. For simplicity, we will call the two CCDs Chip 1 and Chip 2. The image scale is 0.104 arcsec pixel⁻¹.

The observations were obtained with two filters: the on-band filter with a central wavelength of 5025 Å, a FWHM (Full Width Half Maximum) of 60 Å, a peak transmission of 68%, and an equivalent width of 40 Å, and the off-band filter image was done through a standard broadband visual filter. We observed three fields – A, B, and C – centred respectively at $(\alpha, \delta, \text{J2000}) = (0\text{h } 19\text{m } 00.4\text{s}, 59^\circ 16' 25''; 0\text{h } 20\text{m } 03.9\text{s}, 59^\circ 17' 18''; 0\text{h } 20\text{m } 56.9\text{s}, 59^\circ 16' 48'')$, as shown in Figure 1. The observing sequence for each field was: one off-band image (exposure time 150 s), one on-band image (exposure time 1200 s) and two grism+on-band images (exposure time 1200 s). This observing sequence was executed twice for fields A and B and three times for field C.

For the wavelength calibration, after each grism+on-band exposure, an engineering mask was inserted in the light path, and on-band and grism+on-band images were obtained illuminating the mask with the comparison lamp. In addition, on-band and grism+on-band images of the engineering mask were taken illuminating the mask with the Galactic PN NGC 7293 (PNG 036.1-57.1), for radial velocity quality control. Examples of the calibration images are shown in Figure 2 of Méndez et al. (2009). Table 1 shows the log of the observations with the corresponding exposure times and air masses. For brevity, we list only the images corresponding to Chip 1. Identification numbers of Chip 2 images are obtained by adding 1 to the Chip 1 identification numbers in Table 1. The spectrophotometric standard G 138-31 (Oke 1990) was used for the photometric calibration of the on-band images.

2.2 (Re)identification of PNe, FOCAS slitless spectroscopy and Reductions

The traditional on-band/off-band filter technique was used for the re-detection of the known PNe and for the iden-

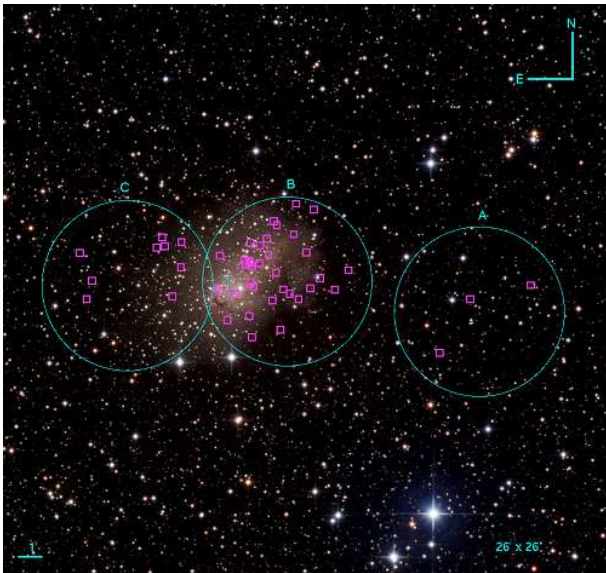


Figure 1. The distribution of all PN candidates (squares) detected with Subaru+FOCAS in IC10. The big circles indicate the 6.5 arcmin FOCAS field of view. At the distance of 660 kpc (see section 4.2), one arcmin corresponds to 0.19 kpc.

Table 1. Journal of observations for Chip 1.

FOCAS Field	Configuration	FOCAS id	Exp	Air Mass
G 138 - 31	On-band	120371	60	1.33
G 138 - 31	On-band	120373	60	1.36
NGC 7293 + mask	On-band	120397	300	1.87
NGC 7293 + mask	On+grism	120399	600	1.80
IC 10 Field B	Off-band	120403	150	1.94
IC 10 Field B	On-band	120405	1200	1.86
IC 10 Field B	On+grism	120407	1200	1.75
IC 10 Field B	On+grism	120409	1200	1.65
IC 10 Field B	Off-band	120423	150	1.46
IC 10 Field B	On-band	120425	1200	1.43
IC 10 Field B	On+grism	120427	1200	1.39
IC 10 Field B	On+grism	120429	1200	1.36
IC 10 Field A	Off-band	120431	150	1.33
IC 10 Field A	On-band	120433	1200	1.32
IC 10 Field A	On+grism	120435	1200	1.31
IC 10 Field A	On+grism	120437	1200	1.30
IC 10 Field C	Off-band	120443	150	1.30
IC 10 Field C	On-band	120445	1200	1.30
IC 10 Field C	On+grism	120447	1200	1.31
IC 10 Field C	On+grism	120449	1200	1.32
IC 10 Field C	Off-band	120451	150	1.33
IC 10 Field C	On-band	120453	1200	1.35
IC 10 Field C	On+grism	120455	1200	1.38
IC 10 Field C	On+grism	120457	1200	1.42
IC 10 Field A	Off-band	120459	150	1.45
IC 10 Field A	On-band	120461	1200	1.48
IC 10 Field A	On+grism	120463	1200	1.54
IC 10 Field A	On+grism	120465	1200	1.62
IC 10 Field C	Off-band	120471	150	1.70
IC 10 Field C	On-band	120473	1200	1.76
IC 10 Field C	On+grism	120475	1200	1.88
IC 10 Field C	On+grism	120477	1200	2.03

tification of new PN candidates. The on-band image is taken through a narrow-band filter passing the redshifted [O III] 5007 Å nebular emission line, while the off-band image is taken through a broader filter passing no nebular emissions. The PNe are visible as point sources in the on-band image, but are absent in the off-band image. A third image, taken through the on-band filter and a grism, confirms the PN can-

Table 2. Radial velocities and magnitudes for the detected PNe in IC10.

ID	α (J2000)	δ (J2000)	RV km s ⁻¹	m_{FOCAS} (5007 Å)	m_{M03} (5007 Å)
01-A	0 18 44.61	59 17 47.83	-328	23.83	24.12 (1)
02-A	0 19 04.40	59 17 04.82	-350	23.63	24.01 (2)
03-A	0 19 13.64	59 14 44.55	-361	23.14	23.58 (3)
04-B	0 19 49.37	59 17 11.08	-371	24.83	-
05-B	0 19 57.71	59 20 31.42	-	26.52	-
06-B*	0 19 57.51	59 17 11.37	-317	24.71	-
07-B	0 19 59.37	59 18 42.11	-361	25.00	-
08-B	0 20 01.15	59 16 41.55	-365	24.87	-
09-B	0 20 03.65	59 20 44.05	-	24.71	-
10-B*	0 20 03.90	59 19 26.12	-323	24.65	-
11-B	0 20 04.20	59 16 55.30	-340	24.18	-
12-B	0 20 06.34	59 17 05.24	-308	25.89	-
13-B	0 20 06.66	59 15 22.18	-354	23.94	24.76 (4)
14-B	0 20 09.68	59 19 47.17	-310	23.83	-
15-B	0 20 09.87	59 16 34.67	-357	25.10	-
16-B	0 20 10.79	59 19 56.67	-344	23.92	-
17-B	0 20 12.75	59 19 11.53	-313	25.73	-
18-B*	0 20 14.74	59 18 08.14	-366	25.60	-
19-B	0 20 14.89	59 18 53.46	-320	24.50	-
20-B	0 20 15.82	59 14 59.75	-333	26.19	-
21-B	0 20 16.21	59 17 07.33	-377	26.22	-
22-B	0 20 17.03	59 17 58.24	-327	24.67	-
23-B*	0 20 17.17	59 15 52.71	-342	23.64	24.49 (5)
24-B	0 20 17.87	59 18 08.72	-365	25.28	-
25-B	0 20 18.00	59 18 11.48	-333	25.69	-
26-B	0 20 18.14	59 18 58.17	-285	25.27	-
27-B	0 20 19.32	59 18 02.70	-324	22.54	-
28-B*	0 20 19.66	59 18 13.03	-341	24.02	-
29-B	0 20 22.28	59 16 46.59	-340	25.23	-
30-B	0 20 24.28	59 15 38.81	-	25.41	-
31-B	0 20 27.58	59 16 53.83	-	26.12	-
32-B	0 20 27.98	59 18 20.91	-	24.78	-
33-C	0 20 40.65	59 17 46.32	-284	-	-
34-C	0 20 40.89	59 18 50.15	-	22.93	23.33 (10)
35-C	0 20 42.95	59 16 30.90	-332	22.85	23.43 (11)
36-C	0 20 46.34	59 18 38.30	-372	26.43	-
37-C	0 20 47.40	59 19 00.05	-284	-	-
38-C	0 20 49.06	59 18 33.16	-279	24.18	-
39-C	0 21 09.80	59 16 59.70	-331	22.81	23.18 (15)
40-C	0 21 11.20	59 16 11.71	-382	23.81	24.52 (16)
41-C	0 21 14.40	59 18 08.17	-303	26.37	-

Notes — (i) The asterisks in the ID column indicate the confirmed PNe studied, through deep medium-resolution optical spectroscopy, by Magrini & Gonçalves (2009). (ii) The last two columns present the magnitudes obtained in this work (m_{FOCAS} , refer to the text for more details) and in Magrini et al. (2003, M03, in which the photometry and astrometry of a number of PN candidates in IC10 were discussed. See their Table 1). In the last column, the numbers in parentheses stand for the M03's IDs.

didates. By inserting the grism in the light path, the images of all continuum sources are transformed into segments of width determined by the on-band filter transmission curve. All the emission-line point sources, such as the PNe, remain as point sources. The grism also introduces a shift relative to the undispersed on-band image which is a function of the wavelength of the nebular emission line and of position on the CCD. By calibrating this shift, we are able to measure the radial velocities for all emission-line objects in the field, as in Méndez et al. (2001, 2009). In the case of Subaru and FOCAS, the dispersing element was an echelle grism with 175 grooves/mm which operates in the 4th order and gives a dispersion of 0.5 Å pixel⁻¹, with an efficiency of 60% (see the Subaru website).

Standard IRAF¹ tasks were used for the basic CCD reductions (bias subtraction, flat field correction using twilight

¹ IRAF is distributed by the National Optical Astronomical Observatories, operated by the Association of Universities for Re-

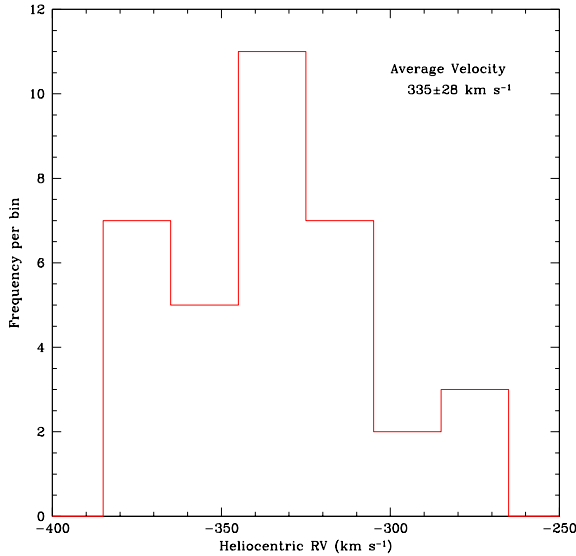


Figure 2. Histogram of heliocentric radial velocities for 35 PN candidates in IC10, in bins of 20 km s^{-1} . The average velocity and dispersion are given in the figure.

flats). We refer the reader to the papers by Méndez et al. (2001, 2009) where a detailed description of all the steps involved in the reduction analysis is given.

3 KINEMATIC ANALYSIS

In Figure 1 we show the spatial distribution of the 41 PN candidates that we have identified in IC10 with Subaru+FOCAS. As explained in Sect. 2.2, we have used the slitless technique to obtain the heliocentric radial velocities (RVs) for the sample. Hereafter, we will refer to our RVs simply as ‘velocities’. Typical images with seeing around $0.5''$ have a point-spread function (PSF) size of 5 pixels, which translates into a radial velocity resolution of 140 km s^{-1} , i.e., the internal velocity field of the PN is not resolved. Assuming position errors of 0.4 pixel, the expected uncertainty in radial velocity is 12 km s^{-1} . However, due to background contamination, bad columns in the images, and the displacement produced by the grism placing some of the sources outside of the fields, we were able to measure the velocities of 35 objects only. The final values are listed in Table 2. Adding quadratically the uncertainties in the velocities, which are given by the calibration errors ($\sim 10 \text{ km s}^{-1}$), the position errors ($\sim 10 \text{ km s}^{-1}$), and the errors from image registration ($\sim 10 \text{ km s}^{-1}$), we get an overall error of about 17 km s^{-1} . Assuming that the spectrograph deformations and guiding errors have a marginal contribution, we estimate the total uncertainty in the velocities measured with Subaru to be at most 20 km s^{-1} .

We show in Figure 2 a histogram of the velocities measured for our targets. There is a clear velocity peak at -335 km s^{-1} , with a dispersion of $\pm 28 \text{ km s}^{-1}$. Within the

uncertainties, the average PN velocity is in good agreement with the NED heliocentric radial velocity of -348 km s^{-1} for IC10. We note from the velocity histogram that none of the objects is apart from the others in terms of velocity distribution. This finding suggests that the objects are true members of IC10.

We then obtained the galactocentric coordinates x and y for the objects. For that purpose we have used a central position of $\alpha(\text{J2000})=0\text{h } 20\text{m } 17.3\text{s}$ and $\delta(\text{J2000})=59^\circ 18' 14''$ for IC10. As IC10 is an irregular galaxy, it is difficult to define its dynamical axis. Wilcots & Miller (1998) argue that even though somewhat uncertain the position angle (PA) value might range between 50 and 90 degrees (see. e.g., their Figure 5). For this reason, we chose to investigate any sign of rotation coming from the PNe along axes with different PA, slightly extending the WM98’s PA range. Along each of those axes we defined four subsamples and calculated the average velocity for each one. We note, however, that the subsamples were not equally spaced in x because we want to ensure a minimum number of PNe per subsample. Figures 3 to 6 show the binned velocities of the PNe along axes with PA of 50° , 60° , 90° and 135° , respectively. We selected these angles because PA= 135° corresponds to the major axis of the IC 10 starlight distribution (as can be seen in Figure 1), while PA= 60° gives the direction along which the neutral gas is rotating, according to SS89 and WM98.

Figures 3, 4 and 5 suggest some rotation along the axis with PA= 50° , 60° and 90° , while figure 6 shows that the evidence of rotation along the optical PA= 135° axis is less significant. We conclude that the PNe (and therefore the stellar population) appear to be rotating like the neutral gas.

Let us make a more detailed comparison. In WM98, the authors produced velocity maps at different locations in the sky, each map corresponding to a velocity channel. In Figure 7 the position of our PNe with velocities falling within the range of the Wilcots & Miller (1998) map channels are superimposed to the corresponding map. We note that in most maps PNe are found to coincide with the gas, further suggesting that the PN kinematics follows the H I one. Note that WM98 concluded, using the velocity maps we just discussed, that their H I velocities followed the rotation curve obtained previously by SS89. So we can also compare our PN velocities to the plots in SS89. In Figure 8 we have taken the position-velocity diagram from SS89 (their Fig. 10) and we have superimposed our PN velocities. This diagram was constructed with an x coordinate measured along PA= 60° , following the observed neutral gas rotation. Along this direction, the H I velocities are very well behaved, as is most clearly seen in SS89’s Fig 8. Turning to our objects, in spite of the high PN velocity dispersion, it is immediately apparent that the PNe are rotating in the same direction, with less negative velocities in the upper left. There is a good overlap with the neutral gas velocities, although several PN velocities are less negative. The full interpretation of this figure is not straightforward, because, although the x coordinates are the same, the y coordinates can be quite different. Consider for example the three PNe in Field A (see Figure 1). Their x coordinates are the most negative in our sample (< -500), and they might be expected to lie at the most negative velocities (they appear at the extreme right of Figure 8); but their average velocity is -340 km s^{-1} .

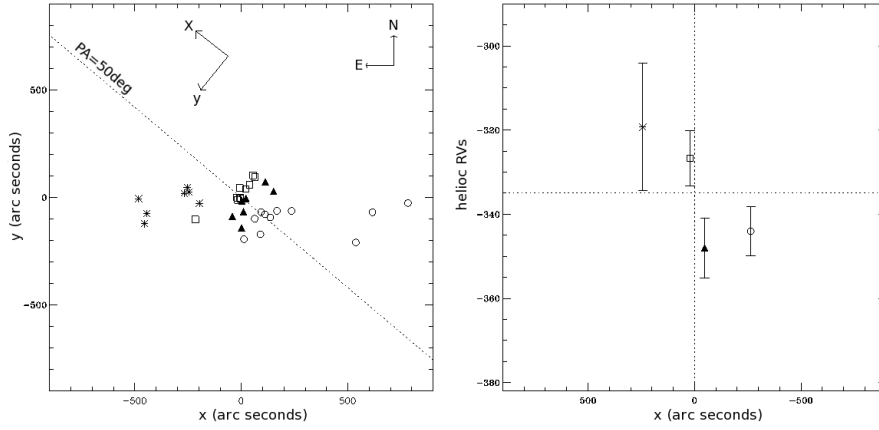


Figure 3. *Left:* the same spatial distribution of PNe as in Figure 1. The dashed line represents an axis of $PA = 50^\circ$. To study the rotation along this axis, the PN sample was divided into four bins perpendicular to it. The orientation of this axis is shown on the top and the PNe inside each bin are represented as: open circles, filled triangles, open squares and stars. *Right:* the average velocity within each bin is plotted at the position of the average x-coordinate of the bin. The 4 bin ranges are: $x < -100''$ (open circle), $-100'' < x < 0''$ (filled triangle), $0'' < x < 100''$ (open square), $x > 100''$ (stars).

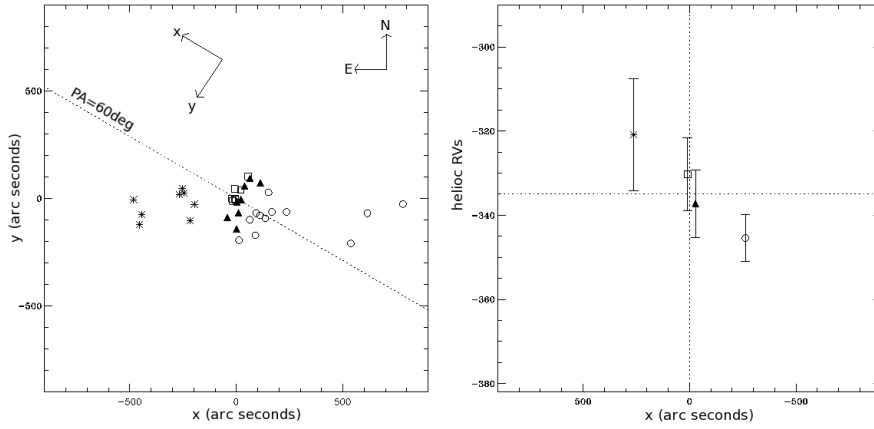


Figure 4. As for Figure 3, except that the rotation is studied along an axis of $PA=60^\circ$.

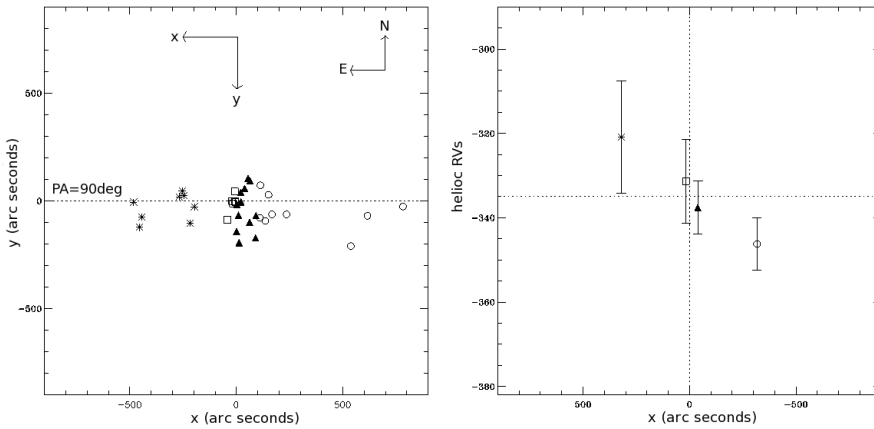


Figure 5. As for Figure 3, except that the rotation is studied along an axis of $PA=90^\circ$.

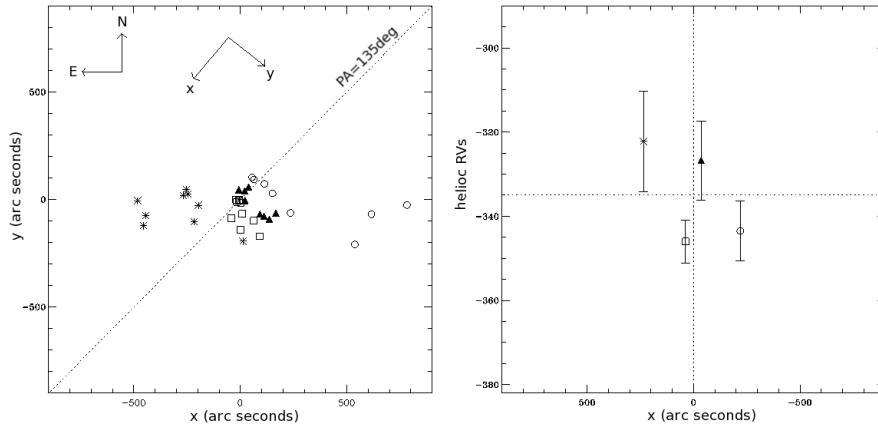


Figure 6. As for Figure 3, except that the rotation is studied along an axis of $PA=135^\circ$.

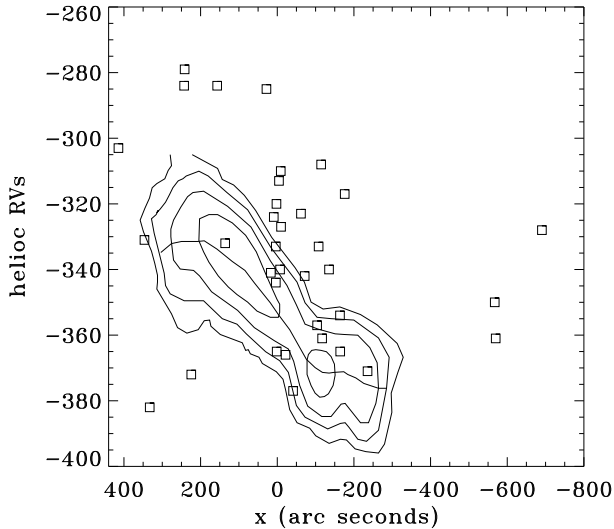


Figure 8. The position-velocity diagram from Figure 10 of SS89, showing the kinematics of neutral gas along $PA=60^\circ$. The squares indicate our PN velocities as a function of the corresponding x coordinate, calculated along an axis with $PA=60^\circ$, as in Figure 4.

However, they should not be compared with the neutral gas velocity distribution shown in Figure 8, because they are in a different part of the sky, to the northwest. In fact, there is a blob of H I close to these Field A PNe, seen in SS89's Fig. 9, and it has a velocity of about -330 km s^{-1} , which fits those few PN velocities quite well, perhaps by chance.

In summary, leaving aside some discrepancies, which probably but not necessarily indicate a tendency toward more negative neutral gas velocity than PN velocities, in Figs. 3 to 8 we have been able to show that most of the PN velocities follow closely the H I kinematics pattern derived by SS89 and WM98. This illustrates the regular, solid-body rotation-like nature of the velocity field (given by the H I as well the PNe) in IC10's disk.

4 PN PHOTOMETRY

A detailed description of the PN photometric procedure is provided by Teodorescu et al. (2010). The results of our photometry for 39 of the 41 objects are listed in Table 2. Two objects (PN 33 and 37) were too close to bright foreground stars, which precluded accurate photometry. The $[\text{O III}] 5007 \text{ \AA}$ fluxes measured through the on-band filter are traditionally expressed in magnitudes $m(5007)$, using the definition introduced by Jacoby (1989).

$$m(5007) = -2.5 \log I(5007) - 13.74. \quad (1)$$

For the flux calibration, we adopted the standard star G138-31 (Oke 1990), which has a monochromatic flux at 5028 \AA (the redshifted wavelength of its $[\text{O III}] 5007 \text{ \AA}$ emission due to the PN radial velocity), of $1.44 \times 10^{-15} \text{ ergs cm}^{-2} \text{ s}^{-1} \text{ \AA}^{-1}$.

If we compare our photometry with that by Magrini et al. (2003) for the objects in common, we find that our values are systematically brighter, by about 0.4 mag. We attribute this to the fact that the nights of Magrini et al. (2003) were not of photometric quality, and thus our new values presented in Table 2 are preferred.

4.1 Foreground extinction

Being located at a low galactic latitude ($l=119.0^\circ$, $b=-3.3^\circ$), IC10 is affected by significant foreground extinction. As previously stated, we find in the literature different values for this parameter. Schlegel, Finkbeiner & Davis (1998) find $E(B - V) = 1.527$, while studies based either on the tip of the red giant branch (TRGB; Sakai et al. 1999; Sanna et al. 2008) or the Cepheids (Wilson et al. 1996) give a range between 0.6 to 1.1 mag. We have adopted $E(B - V) = 0.77$, following Richer et al. (2001), whose extinction value is preferred because of the very convincing work they did, by plotting the reddening as a function of the H I column density in their Figure 3.

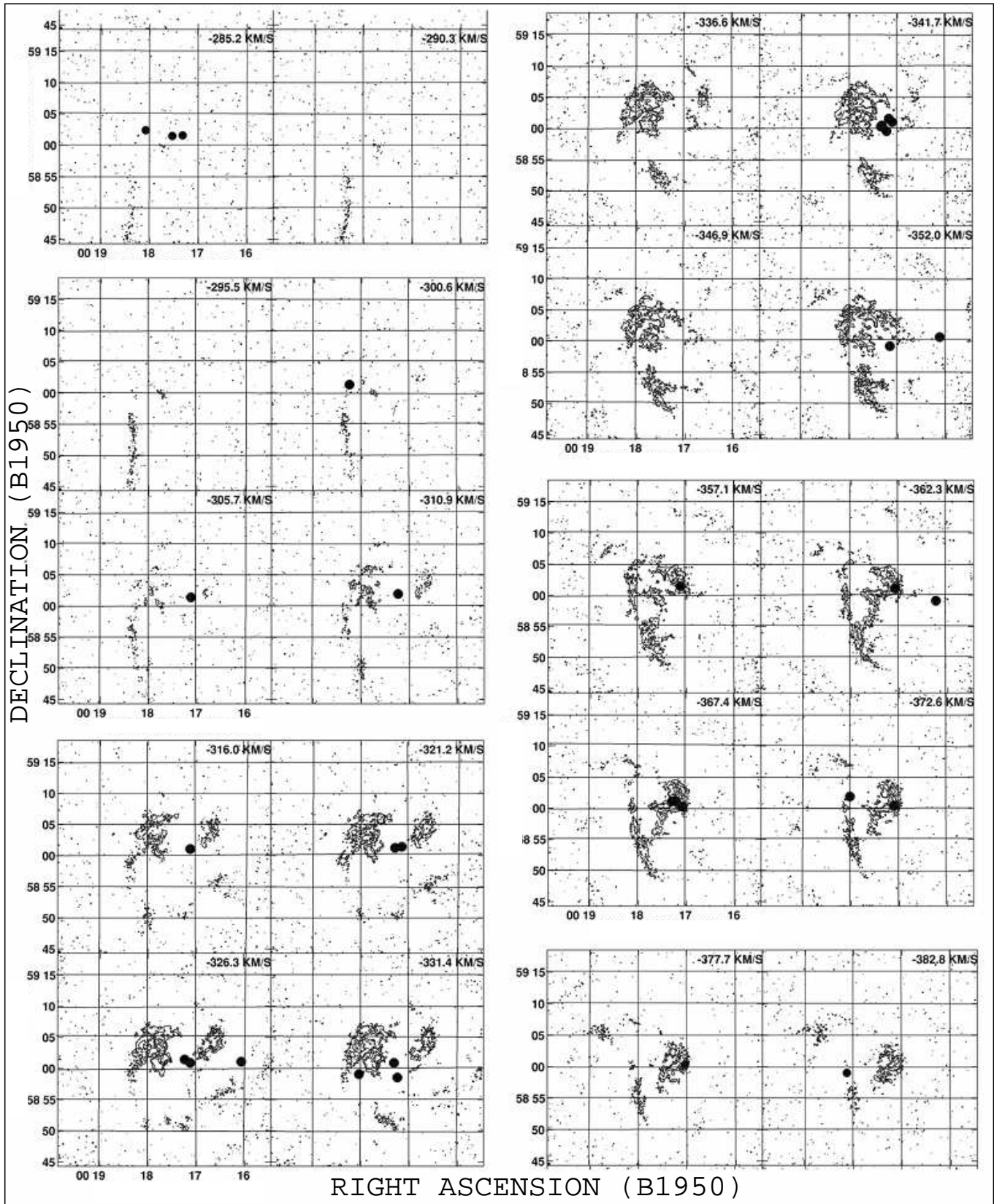


Figure 7. The PN (filled circles) positions superimposed on the H I maps produced by WM98. The velocities of the PNe in each map fall within the velocity range of the map.

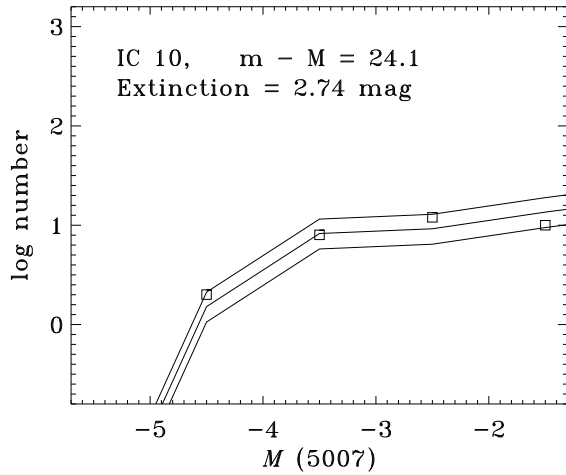


Figure 9. Observed [O III] 5007 PNLF of IC10 (squares), with the sample of 35 PNe binned into 1-mag intervals. The apparent magnitudes $m(5007)$ have been transformed into absolute magnitudes $M(5007)$ by adopting an extinction correction of 2.74 mag and a distance modulus of 24.1. The three lines are PNLF simulations (Méndez and Soffner 1997) for 3 different total PN population sizes: 100, 150 and 200.

4.2 The distance determination from the PN luminosity function

Having measured the apparent magnitudes $m(5007)$ of the 35 PNe, the PN luminosity function (PNLF) was built, using 1-mag bins, and compared with simulated PNLFs like those used by Méndez & Soffner (1997) to fit the observed PNLF of M31. The comparison is shown in Figure 9. The absolute magnitudes $M(5007)$ that produce the best fit to the simulated PNLF were calculated using an extinction correction $A(\lambda)$, at 5007 Å, of $3.56E(B-V)$ (Cardelli et al. 1989), and a distance modulus $(m - M) = 24.1$, which is equivalent to 660 kpc.

The simulated PNLFs plotted in Figure 9 are binned, like the observed one, into 1-mag intervals and have a maximum final mass of $0.63 M_{\odot}$ and sample sizes between 100 and 200 PNe (see Méndez & Soffner 1997; the “sample size” is the total number of PNe, detected or not, that exist in the surveyed area). We selected a rather large bin size of 1 mag to compensate for the rather small number of PNe, and reduce the statistical noise in the PNLF. We estimated an error of 0.2 mag from the goodness of the fit at different distance moduli. To obtain the total error estimate, we have to combine the possible systematic and random errors. The systematic error is the same as in Jacoby et al. (1990), i.e., 0.13 mag, including the possible error in the distance to M31, in the modeling of the PNLF and in the foreground extinction. The random contributions are given by 0.2 mag from the fit to the PNLF, 0.05 mag from the photometric zero point, and 0.05 mag from the filter calibration. Combining all these errors quadratically, we estimate that the total error bar for the PNLF distance modulus is ± 0.25 mag. A PNLF was obtained by Kniazev et al. (2008), based on Magrini et al. (2003) magnitudes. Given the uncertainties in both determinations, Kniazev et al. (2008)’s distance mod-

ulus ($24.30^{+0.18}_{-0.10}$) is in good agreement with ours. Note that we have adopted brighter magnitudes than Magrini et al. (2003). If we correct Kniazev et al. (2008)’s distance modulus by the same amount, their distance modulus decreases to 23.9.

By studying the TRGB in IC10 Sakai et al. (1999) found a distance modulus of 24.1 ± 0.2 mag for Population I and 23.5 ± 0.2 mag for Population II, while Sanna et al. (2008) estimated a distance modulus of 24.57 ± 0.15 mag. From the observations of the Cepheids, Wilson et al. (1996) deduced a distance modulus of 24.57 ± 0.21 mag. Note that there may be some amount of internal extinction in IC10, in addition to the foreground extinction. For the sake of a complete knowledge of the IC10 properties, although not significantly affecting our conclusions about the kinematic pattern of the galaxy, it would be important to know how much extra extinction to expect. Obviously we cannot go further on this discussion without deep individual spectra for all the PNe we found. Such a work, clearly, lies outside of the scope of the present paper. Had we increased the extinction correction to 3.5 mag, equivalent to $E(B - V) = 1.0$ (Demers et al. 2004), our new distance modulus would become 23.3. Such a large correction is unlikely, because many of the objects we discovered are in fact in the outskirts of IC10. We give these numbers to emphasize that the value of the extinction correction is by far the most important source of uncertainty in the PNLF distance determination for IC10.

4.3 PN formation rate

Once the sample size is known, we can calculate the specific PN formation rate $\dot{\xi}$ in units of $\text{PNe yr}^{-1} L_{\odot}^{-1}$:

$$n_{PN} = \dot{\xi} L_T t_{PN}, \quad (2)$$

where n_{PN} is the sample size, L_T is the total bolometric luminosity of the sampled population, expressed in L_{\odot} , and t_{PN} is the lifetime of a PN, for which we have adopted 30,000 yr in the PNLF simulations. We have the B band mag, $B_T = 8.68$, and $B - V = 0.53$, from Richer et al. (2001), and a bolometric correction of -0.8 mag (Buzzoni et al. 2006) from which we obtain an extinction corrected apparent bolometric magnitude 7.35. Using the distance modulus we obtained, of 24.1, and a solar $M_{bol} = 4.72$ we calculate the total luminosity of IC 10, $L_T = 3.9 \times 10^8 L_{\odot}$. The sampled luminosity is 90% of the total luminosity, i.e. $3.5 \times 10^8 L_{\odot}$. Adopting $n_{PN} = 150$ (see subsection above), we get $\dot{\xi} = (14.28 \pm 5) \times 10^{-12}$. Transforming our value of $\dot{\xi}$ into a specific PN density –or α ratio, defined as the number of PNe to the total galaxy luminosity ratio–, as $\log(\alpha) = -6.37$, in agreement with IC10’s starburst quality (Buzzoni et al. 2006 obtained -6.59).

5 DISCUSSIONS

Our motivation to study the PN kinematics of IC 10 is based on the fact that some PN candidates were previously found in this galaxy (Magrini et al. 2003), and, moreover, located at large galactocentric distances (around 3 kpc, see Figure 1) from its centre, PN 1 to 3 in Table 2. The latter can represent a trace of past tidal interactions and/or the connection of the old-intermediate stellar population with the H I envelope

extending 7 times farther than the optical diameter of the galaxy (Huchtmeier 1979; Huchtmeier et al. 1981; see also Meatheringham et al. 1988 for the LCM). So far, no stellar kinematics (of individual objects) was available (for any kind of stars) in IC10, thus the link between stars and gas was missing, and the hypothesis that the H I envelope was a later acquisition, rotating in the opposite direction from that of the inner parts of the galaxy (WM98), needed supporting evidence.

Previous to the present work there have been no kinematic studies of the PN population in IC10. Although IC10 is a dwarf galaxy, where not many PNe can be expected to be found (because of its low luminosity), we were able to collect a sample of 35 PNe. A small sample in absolute terms, but the largest detected to date in this kind of galaxy, with the only exception of the Magellanic clouds (see Table 1 of Magrini 2006, with the number of PNe per LG galaxy, and also Magrini & Gonçalves 2009 and Gonçalves et al. 2012 for an update). It is particularly relevant that PNe form a population with intermediate age between the H I and massive young stars and the old population of red giant stars, and therefore a study of their kinematics should cast light on the problem of the different rotation patterns of the inner disk and its surrounding outer gas (see, e.g., SS89).

The presence of the PN population in the outskirts of IC10 implies that there was active star formation in the outer envelope in the past, several billions of years ago. Unfortunately, without a deep spectroscopic study of the PNe at the outskirts of the galaxy we cannot better date the star formation episode that gave birth to their central stars. Such a study does exist, but only for the central 5.5×5.5 arcmin² region of IC10 (Magrini & Gonçalves 2009). Following the latter authors, the spectroscopically observed PNe, all with low N/O ratio and/or with very low or absent He II, are, to a first approximation, “old stars”. And, thus, they could be born in a limited period of time, 7 to 11 Gyr ago, that is, during the first half of the age of the Universe. This is in agreement with other indications coming from photometric studies of the stellar population in the outskirts of IC 10, e.g., those by Sanna et al. (2009) who identified stars belonging to different star formation episodes (massive young stars (~ 100 Myr), old stars (~ 13 Gyr), and intermediate age stars (~ 0.2 -7 Gyr)). In addition, Sanna et al. (2010) found a significant decrease of the young stellar population when moving from the center toward the outermost regions of IC10. They detected several samples of old red giant stars (well fitted with isochrones of 13 Gyr) up to radial distances of 18-23 arcmin from the galactic center, and an old star excess at least up to 34-42 arcmin from the center. Similar results were also obtained by Tikhonov & Galazutdinova (2009), who detect an old stellar population coincident with the H I envelope. Thus we can suppose that the external PNe are associated with the old and intermediate-age stellar populations, since no young population is detected in the outskirts. Note that we did not detect any H II region in the FOCAS field A, which suggests that, presently, there is no ongoing star formation in the outskirts of IC10. Moreover, being a starburst galaxy, with a current star formation rate ranging from 0.02 to 0.71 $M_{\odot} \text{ yr}^{-1}$ (see Mateo 1998 and Yin et al. 2010 compilations), IC10 is undergoing an intense and very recent burst of star formation (Yin et al. 2010), probably involving only its more central parts. Yin et al. (2010) de-

tailed modelling of IC10 chemical evolution showed, as others previously suspected (Magrini & Gonçalves 2009), that IC10 was probably formed by means of a slow gas accretion process with a long infall timescale of ~ 8 Gyr. This time scale is particularly significant because it corresponds to the epoch of the formation of the PN progenitors in the central regions of IC10. If the progenitors of the PNe located in the outskirts of IC10 had the same age of the central ones, they might be the signature of an epoch of particularly active star formation also in the outskirts of IC10. We might suppose that this important episode of star formation was driven by the first encounter of the H I gas cloud with the IC10 protogalaxy. The conclusions by Sanna et al. (2010) are in very good agreement with our findings, supporting the hypothesis that the H I cloud is associated with IC10 and that it was hosting star formation in the past.

Concluding, the above discussion is in agreement with the numerical simulation by Di Matteo et al. (2007) who investigated the enhancement of star formation efficiency in galaxy interactions and mergers using numerical simulations, and considering different types of encounters, both direct and retrograde. They found that retrograde encounters produce a larger star formation efficiency than direct encounters. They explain this behaviour by the fact that in retrograde encounters tides are less efficient, allowing most of the initial gas to stay in the galaxy, rather than to be driven outwards. This great reservoir of gas can furnish the fuel for an intense burst of star formation in the merging phase.

6 SUMMARY

The study described in this paper was motivated by the fact that a previous search for PNe in IC10 found some PNe located at the outskirts of this starburst galaxy (up to 3 kpc from the centre). Their location by itself suggests that star formation was active in the past at the very outer regions of the galaxy. Thus, we took advantage of the deep imaging and spectroscopic capabilities provided by FOCAS@Subaru to add a number of 29 new objects to the previously known (Magrini et al. 2003; Kniazev et al. 2008; Magrini & Gonçalves 2009) PNe of IC10, simultaneously measuring the radial velocity of most of the galaxy’s PNe.

The average radial velocity of 35 of our PNe is $-335 \pm 28 \text{ km s}^{-1}$, which is, within the errors, the same as the recession velocity of the galaxy (-348 km s^{-1} ; NED). The PN radial velocities were compared with the H I gas velocities in order to examine whether the kinematic connection with the underlying stellar population of IC10 could represent the trace of past tidal interactions in the Local Group. We found that the H I and PN population share the same rotation pattern, as evidenced by the rotation curves along any PA between 50 and 90°, following Shostak & Skillman (1989, and our Figures 3-5 and 8), or the velocity maps of Wilcots & Miller (1998, shown in Figure 7). Moreover, considering that the PNe located at high galactocentric distances in IC10 have roughly the same age as those in the inner regions, around 8 Gyr (Magrini & Gonçalves 2009; Yin et al. 2010), the first encounter of the H I gas with the galaxy can be constrained to have occurred at that time.

Finally, our deep [O III] 5007 Å FOCAS images were used to build up the planetary nebulae luminosity function. From the latter we derived a IC10 distance modulus of 24.1 ± 0.25 , which corresponds to $D = 660$ kpc. This distance is in very good agreement with other recent IC10 distance determinations (Sakai et al. 1999, 24.1 ± 0.2 ; and Kniazev et al. 2008, $24.30^{+0.18}_{-0.10}$).

7 ACKNOWLEDGMENTS

DRG kindly acknowledges the UCL Astrophysics Group, for their hospitality, where part of this work was done. AAB acknowledges support from ARC (Super Science Fellowship, FS110200016). LM is supported through the ASI-INAf grant “HeViCS: the Herschel Virgo Cluster Survey” I/009/10/0. This work was also supported by the National Science Foundation (USA) under grant 0807522.

REFERENCES

- Buzzoni A., Arnaboldi M., & Corradi R. L. M., 2006, MNRAS, 368, 877
- Cardelli J. A., Clayton G.C., & Mathis J.S., 1989, ApJ, 345, 245
- Corradi R. L. M., & Magrini L., 2006, in Proceedings ESO workshop: Planetary Nebulae Beyond the Milky Way, p.36
- Demers S., Battinelli P., & Letarte B. 2004, A&A, 424, 125
- Di Matteo P., Combes F., Melchior A.-L., & Semelin B., 2007, A&A, 468, 61
- Garnett D. R., 1990, ApJ, 363, 142
- Gonçalves D. R., Magrini L., Leisy P. & Corradi R. L. M., 2007, MNRAS, 375, 715
- Gonçalves D. R., Magrini L., Munari U., Corradi R. L. M., & Costa R. D. D., 2008, MNRAS, 391, L84
- Gonçalves D. R., Magrini L., Martins L. P., Teodorescu A. M., & Quireza C., 2012, MNRAS, 419, 854
- Hodge P., & Lee M. G., 1990, PASP, 102, 26
- Huchtmeier W. K., 1979, A&A, 75, 170
- Huchtmeier W. K., Seiradakis J. H., & Materne J. 1981, A&A, 102, 134
- Jacoby G. H., 1989, ApJ, 339, 39
- Jacoby G. H., Ciardullo R., & Ford H. C., 1990, ApJ, 356, 332
- Johnson L. C., Méndez R. H., & Teodorescu A. M., 2009, ApJ, 697, 1138
- Kim M., Kim E., Hwang N., Lee M. G., Im M., Karoji H., Noumaru J., & Tanaka I., 2009, ApJ, 703, 816
- Kashikawa N., et al., 2002, PASJ, 54, 819
- Kniazev A. Y., Pustilnik S. A., & Zucker D. B., 2008, MNRAS, 384, 1045
- Magrini L., Corradi R. M. L., Greimel R., Leisy P. & Lennon D. J., 2003, A&A, 407, 51
- Magrini L., 2006, Planetary Nebulae in our Galaxy and Beyond, Proceedings of the International Astronomical Union, Symposium #234. Edited by Michael J. Barlow and Roberto H. Méndez. Cambridge: Cambridge University Press, p.9
- Magrini L., & Gonçalves D. R., 2009, MNRAS, 398, 280
- Magrini L., Stanghellini L., & Gonçalves D. R. 2011, arXiv:1110.1186
- Massey P., & Armandroff T. E., 1995, AJ, 109, 2470
- Mateo M. L., 1998, ARA&A, 36, 435
- Meatheringham S. J., Dopita M. A., Ford H. C., & Webster B. L., 1988, ApJ, 327, 651
- Melisse J. P. M., & Israel F. P., 1994, A&AS, 103, 391
- Méndez R. H., & Soffner T., 1997, A&A, 321, 898
- Méndez R. H., Riffeser A., Kudritzki R.-P., Matthias M., Freeman K. C., Arnaboldi M., Capaccioli M., & Gerhard O. E., 2001, ApJ, 563, 135
- Méndez R.H., Teodorescu A.M., Kudritzki R.P., & Burkert, A., 2009, ApJ, 691, 228
- Oke J.B., 1990, AJ, 99, 1621
- Richer M. G., Bullejos A., Borissova J., McCall M. L., Lee H., Kurtev R., Georgiev L., Kingsburgh R. L., Ross R., & Rosado M., 2001, A&A, 370, 34
- Sakai S., Madore B. F., Freedman W. L., 1999, ApJ, 511, 671
- Sanna N., Bono G., Stetson P. B., Monelli M., Pietrinferni A., et al., 2008, ApJ, 688, L69
- Sanna N., Bono G., Stetson P. B., Pietrinferni A., Monelli M., et al., 2009, ApJ, 699, L84
- Sanna N., Bono G., Stetson P. B., Ferraro I., Monelli M., et al., 2010, ApJ, 722, L244
- Schlegel D. J., Finkbeiner, D. P., Davis, M., 1998, ApJ, 500, 525
- Skillman E. D., Kennicutt R. C., Hodge P. W., 1989, ApJ, 347, 875
- Shostak G. S., & Skillman E. D., 1989, A&A, 214, 33
- Teodorescu A. M., Méndez R. H., Bernardi F., Riffeser A., Kudritzki R. P., 2010, ApJ, 721, 369
- Thakar A. R., Ryden B. S., Jore K. P., & Broeils A. H., 1997, ApJ, 479, 702
- Tikhonov N. A., & Galazutdinova O. A., 2009, AstL, 35, 748
- White S. D. M., & Frenk C. S., 1991, ApJ, 379, 52
- Wilcots E. M., & Miller B. W., 1998, AJ, 116, 2363
- Wilson C. D., Welch D. L., Reid I. N., Saha A., Hoessel J., 1996, AJ, 111, 1106
- Yin J., Magrini L., Matteucci F., Lanfranchi G. A., Gonçalves D. R., & Costa R. D. D., 2010, A&A, 520, 55

This paper has been typeset from a $\text{\TeX}/\text{\LaTeX}$ file prepared by the author.